International Journal of Precision Engineering and Manufacturing (2026) 27:2969–2983
https://doi.org/10.1007/s12541-025-01388-2

Online ISSN 2005-4602
Print ISSN 2234-7593

REGULAR PAPER

Simple, Commercially Viable Insole Sensor for Simultaneous Plantar Pressure and Shear Stress Measurement Using Tilted Piezoresistive Sensors

Seyong Jung[1] · Quang Van Duong[1] · Juntae Kim[2] · Giuk Lee[3] · Seung Tae Choi[1]

Received: 8 July 2025 / Revised: 11 October 2025 / Accepted: 23 October 2025 / Published online: 27 April 2026
© The Author(s) 2025

Abstract

Accurate measurement of plantar stress is essential for biomechanical monitoring, injury prevention, and clinical diagnosis. While most insole sensors are limited to detecting normal pressure, shear stress, which is critical for assessing postural imbalance and movement dynamics, remains largely unmeasured. This study presents a simple and scalable method to simultaneously measure plantar pressure and shear stress using conventional piezoresistive sensors. Each sensor module consists of five sensors: one centrally placed and oriented parallel to the insole surface and four tilted at 45° in the forward, backward, left, and right directions. The sensors are fabricated on a flexible polyimide substrate and mounted using polyethylene terephthalate film fixtures to maintain their tilted orientations; they are then encapsulated with an ultraviolet-curable (UV-curable) resin for durability. Vertical and shear compression tests were conducted to characterize the orientation-dependent responses of the sensors. Additionally, finite element analysis was performed to verify the positional and orientational changes of the sensors during compression, with results correlated to the experimental data. By analyzing the differential signals from the five sensors, shear stress magnitude and direction were inferred based on characteristic variations in signal output under combined loading. Four sensor modules were embedded into an insole system and tested during treadmill walking and running. The results demonstrated effective, real-time detection of both plantar pressure and shear stress. The system offers a promising solution for gait analysis, athletic-performance monitoring, injury risk assessment, and rehabilitation in both sports and clinical settings.

Highlights

- A simple and scalable insole sensor system is developed using commercial piezoresistive sensors, enabling simultaneous measurement of plantar pressure and shear stress.
- Sensor modules with five distinctly oriented sensors enable direction-sensitive detection of both normal and tangential forces.
- Finite-element analysis is used to accurately determine local stress states on each sensor, accounting for large deformations in elastomeric substrates.
- Experimental results demonstrate reliable discrimination between shear and normal stresses under vertical and inclined loading, as well as during treadmill walking and running.
- The system demonstrates strong potential for real-world biomechanical monitoring, injury prevention, and wearable health applications, owing to its robustness, flexibility, and ease of integration.

Keywords Insole sensor · Piezoresistive sensor · Plantar pressure · Shear stress · Finite-Element analysis · Gait analysis

✉ Seung Tae Choi
stchoi@cau.ac.kr

[1] Functional Materials and Applied Mechanics Lab, School of Mechanical Engineering, Chung-Ang University, Seoul 06974, Republic of Korea

[2] Polyworks Co., Ltd, 238 Bucheon-ro, Wonmi-gu, Bucheon-si 14488, Gyeonggi-do, Republic of Korea

[3] Assistive and Rehabilitation Robotics Lab, School of Mechanical Engineering, Chung-Ang University, Seoul 06974, Republic of Korea

1 Introduction

Plantar pressure and its distribution have been extensively studied across various fields, including foot biomechanics [1–4], athletic performance assessment [5]– [6], disease diagnosis [7–9], and footwear design [10]– [11]. The assessment of plantar stress, which includes both normal (vertical) and shear (tangential) stresses, is essential for understanding human movement, preventing injuries, and addressing medical conditions such as diabetic foot ulcers [9, 12]– [13]. Normal stress reflects the load distribution perpendicular to the foot's surface, whereas shear stress captures tangential forces that can induce friction and tissue distortion. These forces interact significantly in high-load regions such as the heel and metatarsal heads, contributing to injuries, gait abnormalities, and chronic conditions [13–15].

Despite the critical role of shear stress, conventional measurement systems have predominantly focused on normal stress, limiting a comprehensive understanding of plantar mechanics. Honert et al. [4] demonstrated that ground reaction forces (GRFs) estimated from plantar pressure data provide valuable insights into the dynamics of human locomotion. The role of shear stress has gained increasing recognition, particularly for detecting postural imbalances and diagnosing conditions in both sports and medical contexts [6, 9, 15]– [16]. Anterior cruciate ligament tears and ankle sprains, commonly occurring during high-impact movements such as side cuts and crossover cuts, are often associated with excessive internal and external in-shoe shear forces, leading to abnormal joint torques [5, 15]. In the medical domain, the demand for sensors capable of measuring shear stress is growing. For instance, Bader et al. [12] reported that shear stress within subdermal tissues can cause mechanical disruption, contributing to the formation of pressure ulcers.

To address this critical measurement gap, flexible pressure sensors have emerged as key components in e-skin and wearable electronics [17–21]. These sensors are designed to be integrated into insoles for detailed gait monitoring [22]. These insole sensors leverage various transduction principles, primarily piezoresistive, capacitive, piezoelectric, and optical, to measure both normal and shear stress, each presenting a unique combination of advantages and challenges.

Piezoresistive sensors, which function based on the change in electrical resistance of a material under mechanical stress [21, 23–25], are widely utilized. They are known for their high sensitivity, fast response time, and excellent repeatability. For instance, materials like MXene-based composites have demonstrated ultra-high sensitivities up to kPa^{-1} [21], and carbon-based composites have shown excellent stability over thousands of cycles, making them strong candidates for long-term monitoring [17]. Capacitive sensors, conversely, measure pressure by detecting changes in capacitance from the deformation of a dielectric layer. They offer benefits such as a simple structure, good reproducibility, and low power consumption [26]. However, their practical application can be constrained by a limited detection range and durability issues under dynamic loading conditions [13].

For self-powered applications, piezoelectric and triboelectric sensors are prominent. Piezoelectric sensors generate a charge in response to dynamic force or strain [27]– [28], meaning they respond to the rate of change in the applied force. This allows for high sensitivity, but they cannot measure static loads directly and require complex signal processing, such as time integration, to quantify force magnitudes. They also suffer from practical issues like crosstalk and the need for recalibration [28]. Triboelectric nanogenerator (TENG)-based insoles, which generate an AC signal from contact and separation of materials [6, 8, 29], are also self-powered and can measure normal and shear stresses. However, their performance is notably sensitive to environmental conditions like humidity, although encapsulation has been shown to improve durability [8].

Other approaches include optical and inductive sensors [19, 30]– [31]. Optical insoles using fiber Bragg grating (FBG) technology can simultaneously monitor plantar pressure and shear stress by measuring shifts in light wavelength. This method offers a compact and robust solution but requires a complex, individualized calibration procedure for each sensor to achieve accurate force separation [30]. Inductive-based sensors enable tri-axial force measurements but have demonstrated significant durability issues during gait testing, with sensor failure occurring at rapid walking speeds [31].

While these pioneering approaches have significantly advanced the field, they often present practical challenges that limit their widespread adoption. Many existing methods often rely on complex fabrication processes such as photolithography, specialized materials, or the creation of intricate 3D microstructures. Furthermore, accurately decoupling normal and shear forces frequently requires computationally intensive post-processing algorithms, including individualized sensor calibration, phase analysis, or vector decomposition, which can complicate real-time applications. These factors collectively hinder the development of robust, cost-effective, and scalable insole systems suitable for broad clinical and consumer use. This highlights a clear need for a simpler, more accessible method that utilizes commercially available components to reliably measure both plantar pressure and shear stress.

In this study, we propose a simple yet novel sensor array that utilizes conventional piezoresistive sensors to measure both types of stress. The sensor array consists of five

piezoresistive sensors: one aligned parallel to the insole surface and four tilted at 45° in forward, backward, left, and right directions. This configuration enables differential signal analysis to distinguish between normal and shear stresses. The sensors are fabricated on a flexible polyimide substrate using standard manufacturing processes. Polyethylene terephthalate (PET) films serve as simple mechanical fixtures to maintain the inclined orientations, and encapsulation with ultraviolet (UV)-curable resin provides structural robustness. We conducted vertical and shear compression tests to evaluate the voltage–stress responses of the sensors and employed finite element analysis (FEA) to validate their performance under various loading conditions. Insole modules incorporating four modules of these sensors were fabricated and tested during treadmill walking and running. The results demonstrated effective measurement of both normal and shear stresses, indicating the potential of this technology for motion tracking, athletic-performance evaluation, injury prevention, and health monitoring. Importantly, the simplicity and commercial viability of this design could facilitate its widespread adoption in both clinical and athletic settings.

2 Design and Fabrication of Piezoresistive Sensor Arrays

2.1 Design and Sensing Mechanism

We propose a method for measuring plantar pressure and shear stress using a commercial piezoresistive sensor (PAG array sensor series) developed by Polyworks Co. (Republic of Korea). The top and cross-sectional views of this commercial piezoresistive sensor are shown in Figs. 1(a) and 1(b), respectively. The sensor is fabricated on a 180 μm-thick flexible printed circuit board (FPCB), comprising a top layer of PET film, a piezoresistive material, a pair of electrodes, and a bottom layer of polyimide (PI) film. The piezoresistive material is a composite of carbon black and epoxy. Similar to conventional piezoresistive sensors, when a normal pressure is applied, the pair of electrodes is pressed against the piezoresistive material, causing a change in electrical resistance proportional to the applied pressure. This mechanism enables accurate pressure measurement based on resistance variation.

A simple method for measuring shear stress using the piezoresistive sensor is illustrated in Fig. 1(c). In this illustration, both a normal stress (p_a) and a shear stress (τ_a) are applied to the substrate, where the subscript "a" denotes externally applied stresses. Three piezoresistive sensors are arranged such that their sensing surfaces are oriented in three distinct directions: normal to the surface (N), tilted to the left (L), and tilted to the right (R). Owing to these differing orientations, the normal and shear stresses acting on each sensor vary, leading to distinct output signals. The externally applied normal and shear stresses (p_a and τ_a) can be estimated by analyzing the differences among the three sensor outputs.

The normal stress (σ^s_{22}) and shear stress (τ^s_{12}) acting on each sensor, in the local coordinate system attached to the sensor (denoted by the superscript "s"), can be expressed using the following stress-transformation equations:

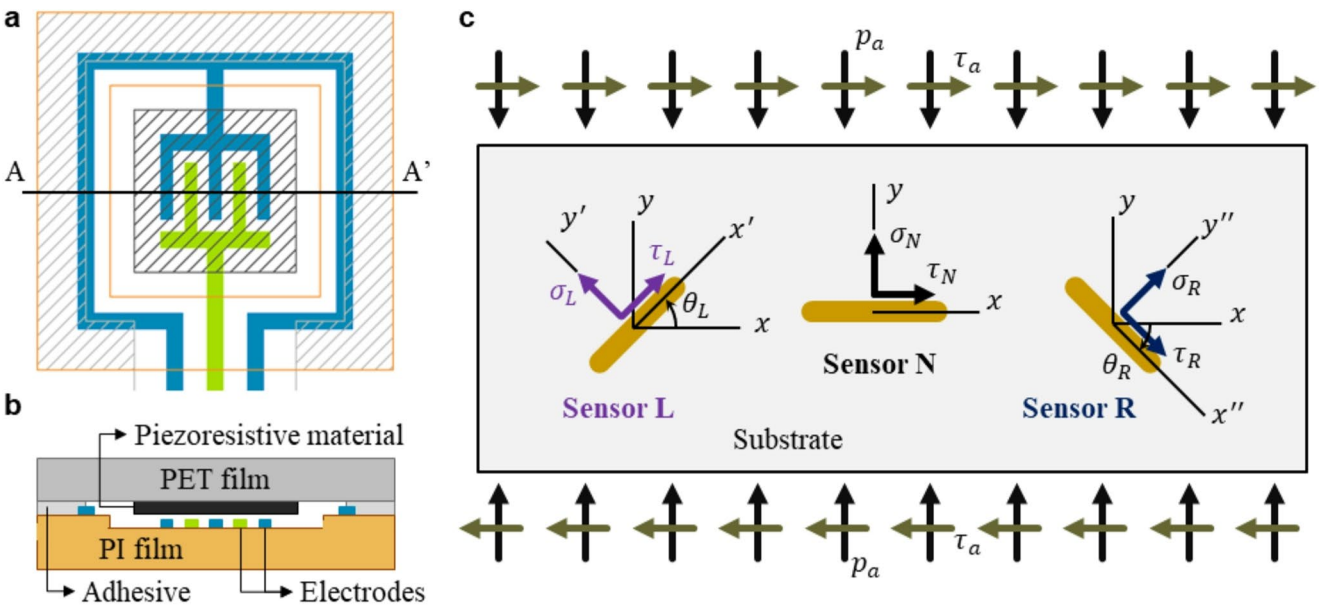


Fig. 1 **a** Design of a piezoresistive sensor; **b** cross-sectional view along the AA' line of the piezoresistive sensor; **c** concept of measuring normal and shear stresses using an array of piezoresistive sensors

$$\sigma_{22}^{s} = p_a/2 + (p_a/2)\cos(2\theta) - \tau_a \sin(2\theta) \quad (1)$$

$$\tau_{12}^{s} = (p_a/2)\sin(2\theta) + \tau_a \cos(2\theta) \quad (2)$$

where the normal stress parallel to the substrate is assumed to be zero. However, when the substrate is made of an elastomer, large deformations may occur under the applied stresses, causing the actual stresses on the sensor to deviate from the values predicted by these transformation equations, which are based on linear elastic, small deformation theory. Therefore, a more general functional form of stress transformation is required:

$$\sigma_{22}^{s} = f_n(p_a, \tau_a, \theta) \quad (3)$$

$$\tau_{12}^{s} = f_s(p_a, \tau_a, \theta) \quad (4)$$

The stress-transformation functions f_n and f_s are determined through FEA, as discussed in Sect. 3.

A critical challenge addressed in this study is that the piezoresistive sensor responds to both normal and shear stress, generating voltage signals under both types of loading. This characteristic complicates stress analysis, as the sensor output cannot be attributed to a single stress component. Instead, the sensor response is modeled as a characteristic function that depends on both stress components:

$$V = g(\sigma, \tau) \quad (5)$$

where $g(\bullet)$ represents the intrinsic response function of the sensor, determined through independent calibration experiments. Using this function, the externally applied normal and shear stresses (p_a and τ_a) can be estimated from the output voltages of the three differently oriented sensors (V_N, V_L, and V_R).

2.2 Fabrication of a Sensor Module

This section describes the fabrication of a sensor module that incorporates tilted sensors, using a commercial piezoresistive sensor developed by Polyworks Co., Ltd., to enable the simultaneous measurement of normal and shear stresses. Each sensor module comprises five piezoresistive pressure sensors, as shown in Fig. 2(a). The sensor holder is fabricated from PET film, as indicated by the blue lines in Fig. 2(b), and includes a 6-mm diameter central hole with four surrounding slits, each 7.8 mm in length. Each sensor, whose outer shape is represented by the red lines in Fig. 2(b), is bent and inserted into these four slits. As shown in Fig. 2(c), a single sensor becomes tilted at a 45° angle when inserted into the PET holder. The central hole in the PET holder is designed to transmit externally applied stress directly to the sensor, minimizing interference from the holder.

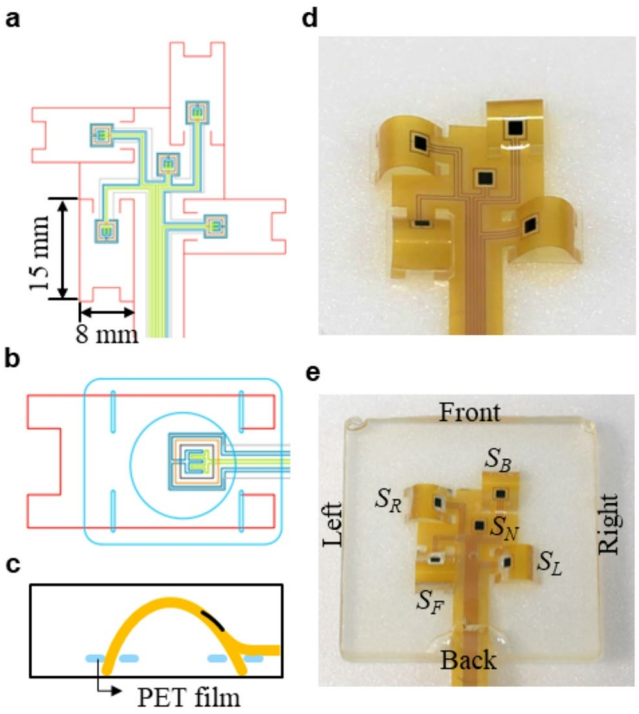


Fig. 2 **a** Technical drawing showing the layout of the piezoresistive sensor array with one central sensor and four tilted sensors; **b** technical drawing of the PET holder (shown in deep sky blue) with a central hole and four slits for fixing sensor orientation; **c** illustration of a piezoresistive sensor tilted at 45° using the PET holder; **d** photograph of a sensor module assembled with PET holders before encapsulation; **e** photograph of a fully molded sensor module after UV-curable elastomer encapsulation

Figure 2(d) shows a completed sensor module in which four sensors are tilted in four different directions, while the central sensor remains parallel to the surface. The sensor module is encapsulated in SuperElastic (ENGR-E38L, 3DMaterials Co., Republic of Korea), a UV-curable resin, and cured under a UV lamp for 1 h. The resulting module has dimensions of 50 × 50 × 6 mm, as shown in the photograph in Fig. 2(e). The four sensors for measuring shear stress are arranged in a 2 × 2 array with 20-mm spacing, while the sensor for measuring normal stress is positioned at the center of this array. Ideally, both normal and shear stresses should be measured at the same location; however, owing to physical constraints, the shear-stress sensors are positioned approximately 14 mm from the central normal-stress sensor. The subscripts N, L, R, F, and B are used to denote the orientation of each sensor's surface-normal vector: N for normal to the surface, L for left-tilted, R for right-tilted, F for forward-tilted, and B for backward-tilted. These subscripts are consistently applied to identify each sensor (e.g., S_N) and their corresponding output signals (e.g., V_N).

2.3 Fabrication of an Insole Sensor

The insole-type sensor is designed for a foot size of 270 mm and incorporates four sensor modules positioned at the big toe (T), first metatarsal head (1MH), fifth metatarsal head (5MH), and heel (H), as shown in Fig. 3(a). These locations are biomechanically significant, as they correspond to regions of peak plantar pressure during key phases of the gait cycle, such as heel strike, mid-stance, and toe-off, enabling comprehensive monitoring of dynamic foot loading patterns. To prevent air entrapment, which could interfere with sensor performance, the FPCB structure is equipped with three air vents located at the forefoot, midfoot, and heel regions. Additionally, the signal lines are routed near the ankle to allow direct and unobtrusive connection to external electronics during walking or running. The sensor modules are integrated into the final insole by being molded with SuperElastic, a UV-curable elastomeric polymer. The resulting flexible insole has a final thickness of 6 mm, a design which ensures both structural protection and user comfort during extended wear, as shown in Fig. 3(b). The soft, UV-curable elastomer provides structural protection while preserving comfort during extended wear. Furthermore, this fabrication process, which utilizes commercially available piezoresistive sensors, was designed for repeatability and scalability for potential commercial applications.

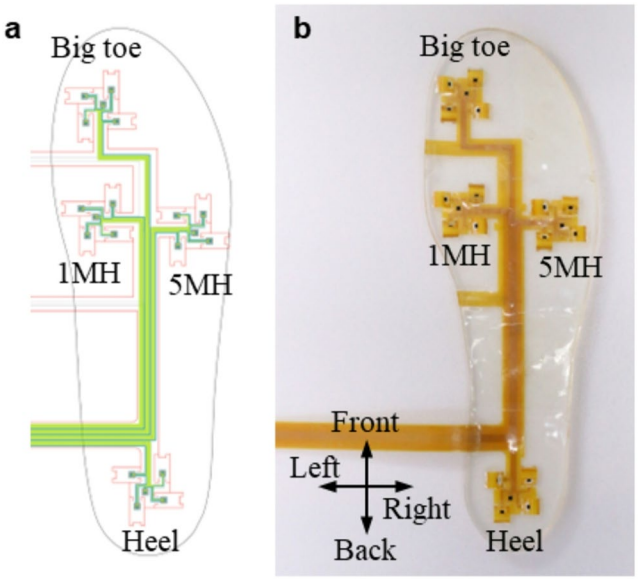


Fig. 3 **a** Technical drawing of the insole-type sensor array showing the placement of four sensor modules; **b** photograph of the fabricated insole integrated with the sensor array

3 Estimation of Stress-Transformation Functions Via FEA

To analyze the stress distribution and displacement within the piezoresistive sensor embedded in the sensor module, an FEA was conducted using ABAQUS software [32]. The objective of this analysis is to estimate the stress-transformation functions defined in Eqs. (3) and (4), which relate externally applied normal and shear stresses to the local stresses experienced by the five piezoresistive sensors. As discussed in Sect. 2, when the substrate is an elastomer, large deformations may occur under applied loads. These deformations can cause significant rotations, particularly in the tilted sensors, leading to discrepancies between the actual sensor stresses and those predicted by conventional stress-transformation equations (Eqs. (1) and (2)), which are based on linear elastic small-deformation theory. To account for such nonlinear effects and to accurately estimate the local stresses, FEA is employed in place of purely analytical methods. Specifically, the nonlinear geometry option was enabled in the FEA to incorporate large deformation behavior.

Simulations were performed under two distinct loading conditions: (1) vertical compression (representing pure normal stress) and (2) combined loading (which includes both normal and shear stress components). For each scenario, three sensor orientations are analyzed: one parallel to the substrate surface (S_N), one tilted to the left (S_L), and one tilted to the right (S_R). Figures 4(a) and 4(b) illustrate the simulation models under vertical compression and combined loading conditions, respectively. In the combined loading case, compression is applied at a 45° angle to simulate the simultaneous effects of p_a and τ_a.

The mechanical properties of the elastomeric substrate (SuperElastic) were characterized via uniaxial tensile testing using a universal testing machine (Ametek LS 5, Lloyd Instruments, England). Full-field deformation was captured using digital image correlation, and the resulting stress–strain curve, shown in Fig. 4(c), yielded a Young's modulus of 2.6 MPa and a Poisson's ratio of 0.4. The Young's modulus and Poisson's ratio of both the piezoresistive pressure sensor and the PET film were assumed to be 2.5 GPa and 0.4, respectively. In the FEA, contact interactions were defined using a hard contact in the normal direction and the penalty method in the tangential direction, with a friction coefficient of 0.25. The bottom surface of the sensor module was fully constrained, and compression was applied from the top via a rigid jig, which was displaced downward by 0.9 mm for the vertical loading case and 1.2 mm for the combined loading case.

Figure 4(d) shows the undeformed and deformed shapes of the S_L sensor under vertical compression, along with the

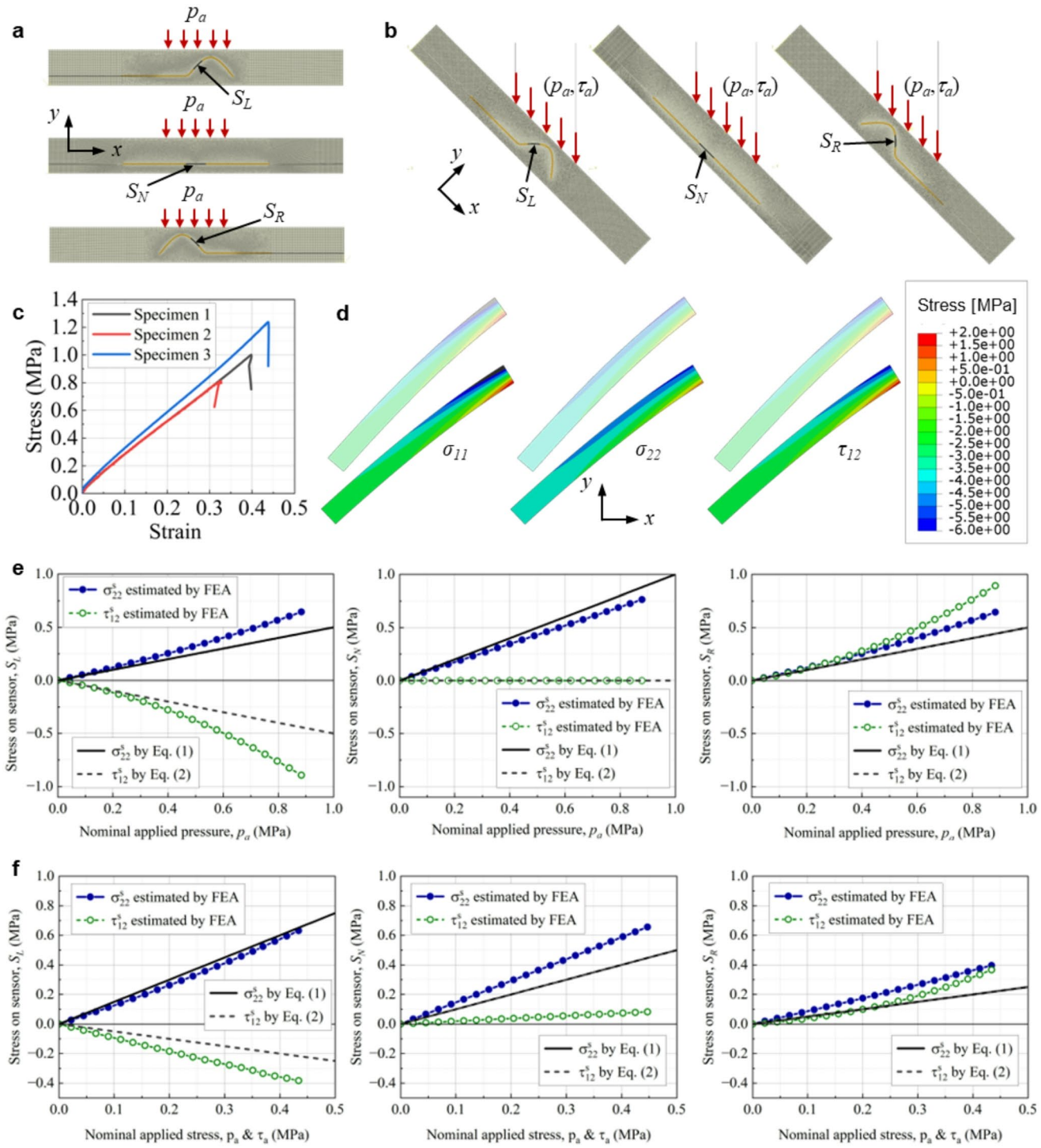


Fig. 4 FEA results for the sensor module under vertical and 45° shear compression: geometry of the S_L, S_N, and S_R sensors under **a** vertical compression and **b** 45° shear compression; **c** measured stress–strain curve of the elastomer substrate (SuperElastic); **d** deformation and distribution of σ_{11}, σ_{22}, and τ_{12} in the S_L sensor under vertical compression; average normal stresses on the S_L, S_N, and S_R sensors as a function of nominal applied pressure under **e** vertical compression and **f** shear compression

corresponding stress components (σ_{11}, σ_{22}, and τ_{12}). The sensor's orientation angle decreased from an initial 44° to approximately 38.4°, indicating a rotation of 5.6° due to the applied load. Under combined loading, the rotation angles for the S_L, S_N, and S_R sensors were observed to decrease by 7.5°, 1.5°, and 2.4°, respectively. Using the stress fields obtained from the FEA, average normal and shear stresses acting on the three sensors (S_L, S_N, and S_R)

were calculated. These values are presented in Fig. 4(e) for vertical compression and Fig. 4(f) for combined loading. For comparison, the analytically predicted stresses based on Eqs. (1) and (2) (assuming linear elasticity and small deformation) are also plotted using solid and dashed lines.

Under pure vertical compression, the shear stress component in the S_N sensor was nearly zero, while the normal stress was marginally lower than that predicted by Eq. (1), likely owing to partial attenuation of the applied pressure p_a as it was transmitted through the elastomeric substrate. For the tilted sensors (S_L and S_R), the stress profiles were symmetric, except for the opposing signs of the shear components. Although p_a and τ_a had the same nominal magnitude in the combined case, the FEA results revealed that both σ^s_{22} and τ^s_{12} in the tilted sensors exceeded their nominal values. This discrepancy was attributed to large deformation and the resultant rotation and distortion of the sensor elements.

Under combined loading, the FEA-predicted σ^s_{22} in the S_N sensor was higher than the applied p_a, whereas the corresponding τ^s_{12} was significantly lower than the applied τ_a. For the S_L sensor, which is oriented nearly perpendicular to the direction of the applied traction, a large normal stress σ^s_{22} developed, accompanied by an increasing shear stress τ^s_{12} as deformation progressed. In contrast, the S_R sensor, which is nearly aligned with the traction direction, exhibited the lowest normal stress among the three.

Crucially, the average stresses calculated for each sensor and presented in Figs. 4(e) and 4(f) directly represent the stress-transformation functions f_n and f_s defined in Eqs. (3) and (4). Rather than formulating explicit equations or constructing lookup tables, the FEA-derived curves themselves serve as effective calibration functions. These functions enable accurate estimation of the local stresses experienced by each sensor based on known external loads during experimental testing, as further discussed in Sect. 4. The FEA results provided in Fig. 4 thus form the essential foundation for determining the sensor's voltage response function $g(\sigma, \tau)$ described in Sect. 4. Specifically, the local stress values obtained from Figs. 4(e) and 4(f) will be mapped to the corresponding sensor output voltages obtained experimentally, facilitating the practical determination and application of the sensor's characteristic function $g(\sigma, \tau)$.

4 Sensor Characterization and Performance Evaluation

4.1 Experimental Setup for Vertical and Shear Compression Tests

The sensor modules were evaluated using a uniaxial mechanical testing machine (T&DORF Inc., Republic of Korea) equipped with a 500 N load cell. The vertical compression test setup is shown in Fig. 5(a) (schematic) and Fig. 5(b) (photograph), where the sensor module is placed flat on a bottom plate parallel to the ground. A cylindrical top jig with a diameter of 10 mm was used to apply vertical compression. The shear compression test setup is shown in Fig. 5(c) (schematic) and Fig. 5(d) (photograph). The sensor module was placed on a bottom jig inclined at either 30° or 45°, with the front side of the module facing down the slope. The top jig used to apply compression at an angle was fabricated by cutting a 10 mm diameter cylinder at 30° or 45°, matching the slope of the bottom jig. To calculate the nominal applied pressure, the force measured by the load cell was divided by the cross-sectional area of the top jig.

Each of the five piezoresistive sensors in the module was tested individually, and their voltage outputs were recorded as the nominal pressure was increased from 0 to 1000 kPa at a loading speed of 10 μm/s. While the FEA in Sect. 3 considered only two tilted sensors (S_L and S_R) owing to the two-dimensional simulation domain, the actual sensor module is three-dimensional. Therefore, in the mechanical tests, all five sensor configurations, including the center sensor

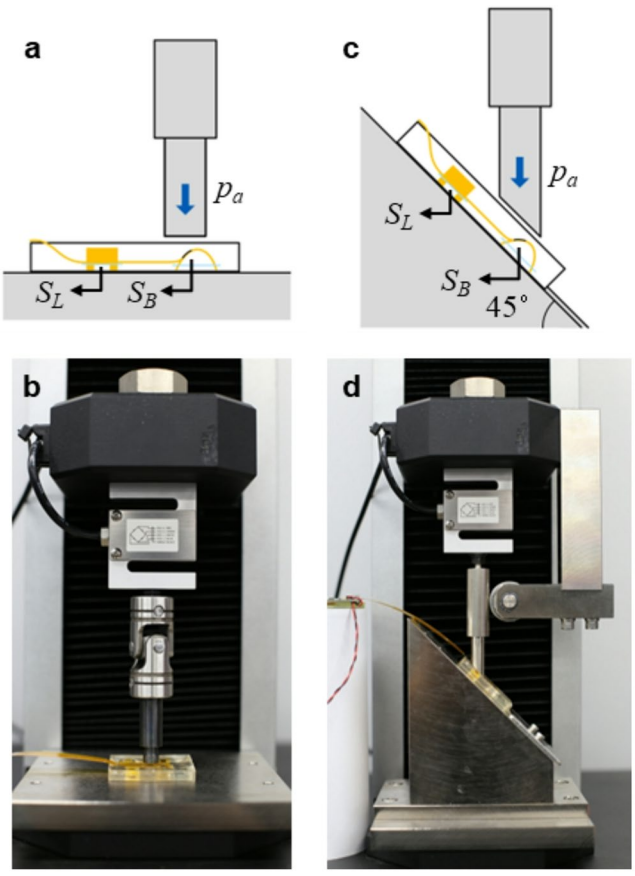


Fig. 5 **a** Schematic and **b** experimental setup of vertical compression test; **c** schematic and **d** experimental setup of shear compression test

(S_N) and the four tilted sensors (S_L, S_R, S_F, and S_B), were evaluated to fully characterize the directional response of the module under both vertical and shear loading.

4.2 Performance Evaluation of Shear Stress and Plantar Pressure Sensors

Figure 6 shows the results of the vertical and shear compression tests performed on the sensor modules. In the vertical compression test (Figs. 6(a) and 6(b)), the S_N sensor, which is aligned parallel to the surface, exhibited significantly higher sensitivity, with measurable output beginning at a nominal pressure as low as 10 kPa. Specifically, the S_N sensor shows a linear response in two distinct regions as indicated in Fig. 6(a): one with a slope of 11.54 mV/kPa in the 0–100 kPa range, and another with a slope of 1.99 mV/kPa in the 100–1000 kPa range. This indicates that the sensor is approximately six times more sensitive at lower pressures than at higher pressures. In contrast, the tilted sensors (S_L, S_R, S_F, and S_B) began producing measurable outputs only at higher nominal pressures, ranging from 250 to 350 kPa. The distinct difference in initial response and sensitivity between the vertically oriented S_N sensor and the tilted sensors clearly indicates that sensor orientation strongly influences sensitivity to normal pressure.

In the shear compression tests conducted at a 30° inclination (Figs. 6(c) and 6(d)), the sensors exhibited direction-dependent output characteristics. Specifically, the S_L sensor began detecting output at a nominal pressure of approximately 220 kPa, while the S_F and S_B sensors responded at approximately 350 kPa. Notably, the S_R sensor had the highest detection threshold, with output beginning at approximately 540 kPa. Furthermore, compared to the vertical compression condition, the output of the S_R sensor decreased considerably under 30° inclined shear loading. This behavior is consistent with the S_R sensor's orientation, which is nearly parallel to the direction of applied load, resulting in reduced effective normal stress on the sensor surface.

At a higher shear angle of 45° (Figs. 6(e) and 6(f)), the direction-dependent behavior of the sensors became more pronounced. The nominal pressures at which output was detected were approximately 200 kPa for the S_L sensor, 350 kPa for the S_F and S_B sensors, and 650 kPa for the S_R sensor. The increased onset pressure for the S_R sensor under 45° loading compared to 30° further highlights its reduced sensitivity when aligned with the direction of the applied shear. Consequently, the difference in output between sensor pairs located opposite each other (e.g., S_L vs. S_R) became more prominent with increasing shear angle, indicating a high degree of directional sensitivity. This suggests strong potential for discriminating shear load directions.

A noteworthy characteristic of the system is observed in the response of the normally-oriented S_N sensor. As the loading condition was varied from pure vertical compression (Fig. 6(b)) to shear compression at 30° (Fig. 6(d)) and 45° (Fig. 6(f)), the ratio of normal to shear stress applied

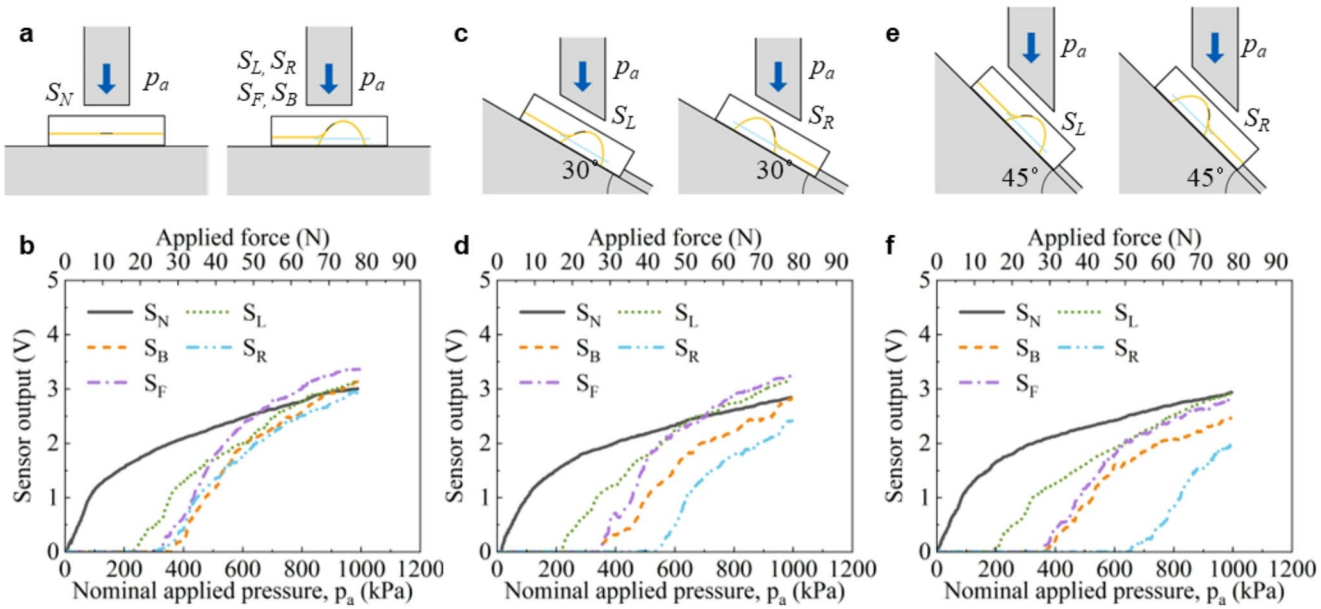


Fig. 6 **a** Schematic of the vertical compression test; **b** sensor output voltages as a function of nominal applied pressure during the vertical compression test; **c** schematic of the 30° shear compression test; **d** sensor output voltages as a function of nominal applied pressure during the 30° shear compression test; **e** schematic of the 45° shear compression test; **f** sensor output voltages as a function of nominal applied pressure during the 45° shear compression test

to the module changed significantly. Despite the sensor's inherent sensitivity to both stress components, as stated in Sect. 2.1, the experimental results uniquely show that its output remained remarkably consistent for the same nominal applied pressure (p_a) across all three test conditions.

As shown in the shear test results on an inclined plane tilted along the L-R axis (Figs. 6(d) and 6(f)), the S_L and S_R sensors exhibited a distinct differential response corresponding to the shear direction. Concurrently, the orthogonally positioned S_F and S_B sensors produced outputs with only a minimal deviation from their behavior under pure normal compression, which confirms the sensor module's ability to selectively detect the direction of the applied shear force. Due to the module's symmetrical design, a test along the F-B axis was omitted for brevity, as it would be redundant; the shear-detecting roles of the F-B sensor pair (S_F and S_B) and the L-R sensor pair (S_L and S_R) would simply be interchanged.

As described in Sect. 3 (Fig. 4), the FEA simulation provides stress-transformation functions that enable the correlation of the nominal applied pressures used in the experiments (such as those shown in Figs. 6(b) and 6(f)) with the local normal and shear stresses acting on the sensor surfaces. Therefore, for a known nominal pressure, loading condition (vertical or 45° shear), and sensor orientation, the local stresses (σ^{s}_{22} and τ^{s}_{12}) can be obtained from the FEA results in Figs. 4(e) and 4(f). By pairing these local stresses with the experimentally measured voltage outputs, the intrinsic sensor characteristic function $V = g(\sigma, \tau)$ can, in principle, be determined. While this study did not implement a complete calibration procedure to convert measured voltages into exact stress values, the presented results successfully demonstrate the feasibility of developing such a function. A detailed, quantitative determination of the sensor characteristic function $g(\sigma, \tau)$ is designated for future work.

Overall, these experimental findings confirm that sensor orientation significantly influences the response of piezoresistive elements under combined normal and shear loads. Importantly, this orientation-dependent behavior provides a practical basis for distinguishing shear directions, enhancing the applicability of the sensor system for comprehensive plantar stress analysis in real-world biomechanical monitoring scenarios.

To evaluate the repeatability of the sensor modules, a cyclic vertical compression test was performed on the vertical sensor (S_N) and a tilted sensor (S_R) for 100 cycles with a load ranging from 0 to 380 kPa. As shown in Fig. 7, the results indicate distinct behaviors for each sensor orientation. In the case of the S_N sensor, the sensor output exhibited viscoelastic-like behavior, where the sensor output showed significant initial drift and gradual stabilization over time. A drift of approximately 10% was observed over 100 cycles (approximately 4000 s). For the S_R sensor, the output showed a relatively large deviation in the initial cycles but demonstrated good repeatability within 7% after 20 cycles.

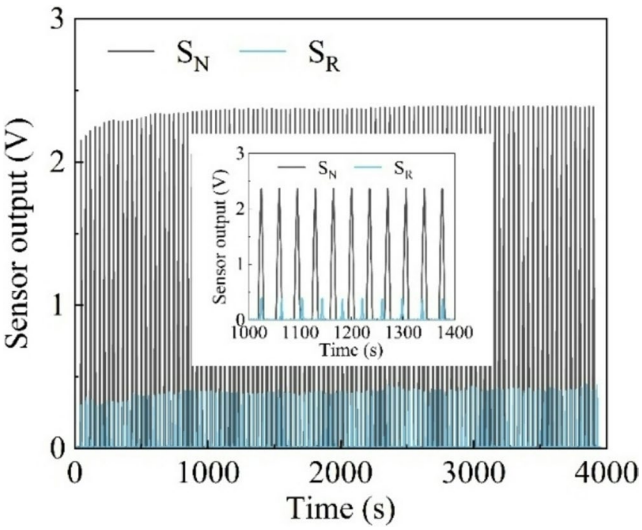


Fig. 7 Repeatability test of the sensor modules under cyclic vertical compression. The plot shows the output signals from the normally-oriented sensor (SN) and a tilted sensor (SR) over 100 cycles of loading and unloading (0–380 kPa)

5 Experimental Validation in Gait Analysis

5.1 Static Characteristics with Different Standing Postures

In this section, an insole sensor system inserted into the right shoe was evaluated under three different static standing conditions: standing on flat ground (0°), standing on a 10° incline, and standing on a 20° incline (Fig. 8(a)). These postures were selected to systematically investigate the impact of surface slope on the outputs of both normal and tilted sensors, reflecting variations in plantar pressure (normal stress) and shear stress under static conditions. A printed circuit board (POLYWORKS©, Republic of Korea) and a data acquisition system (USB-6343, National Instruments, USA), customized for insole-type sensor arrays, were used to record sensor signals.

Figure 8(b) shows the outputs from sensor modules located at four key regions of the insole: the big toe (T), first metatarsal head (1MH), fifth metatarsal head (5MH), and heel (H). When standing on a flat surface (0° incline), the dominant outputs came from the normal-oriented sensors at the big toe (T_N) and heel (H_N). No measurable output was observed at the first and fifth metatarsal regions, indicating

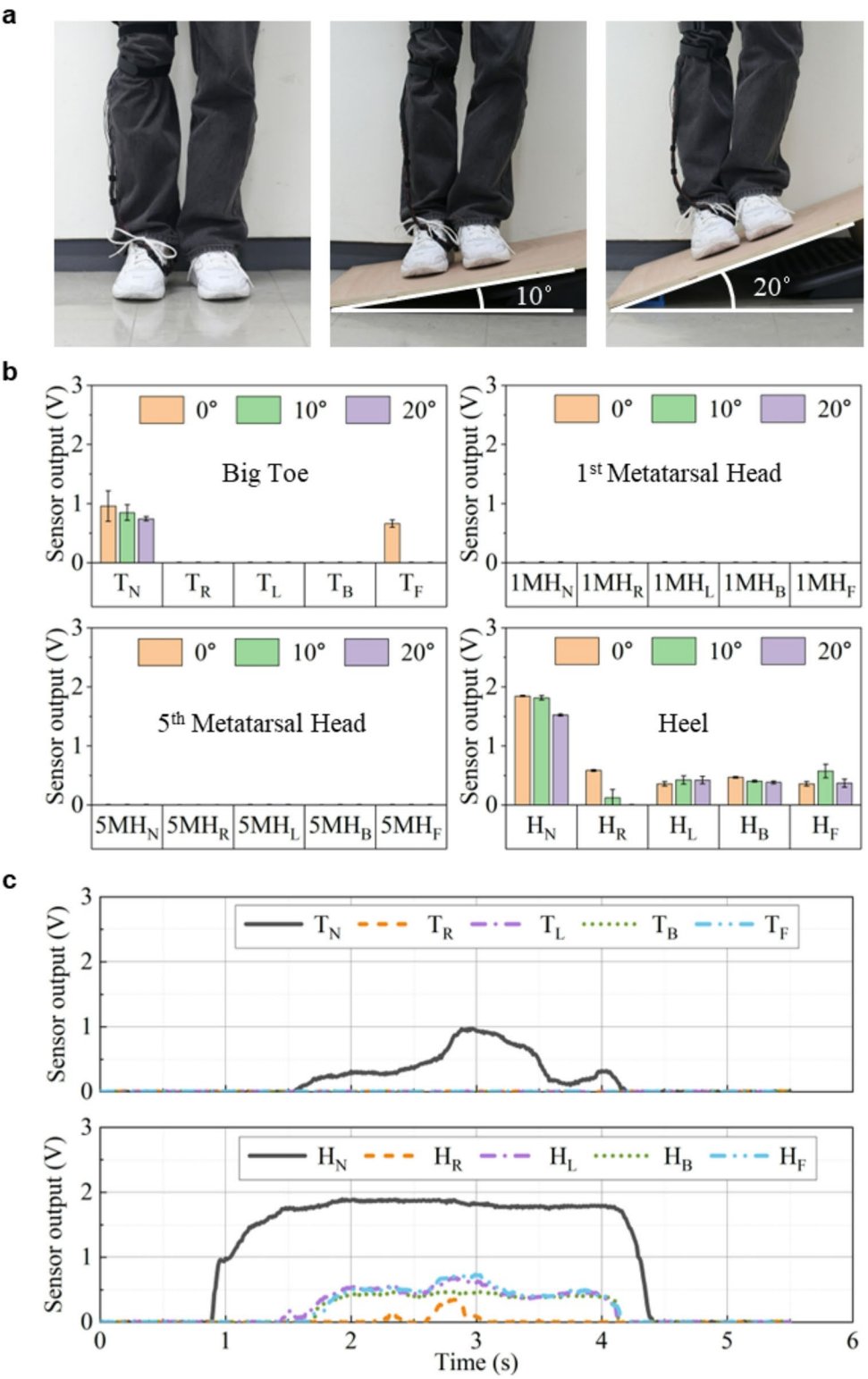


Fig. 8 **a** Photographs of three static standing postures: flat ground (0°), 10° left-right (LR) tilt, and 20° LR tilt; **b** sensor output voltages under 0°, 10°, and 20° LR tilt conditions at each sensor location; **c** time-resolved sensor output voltages at the big toe and heel positions during in-place stepping on a 20° LR tilt

minimal plantar loading in these areas during static standing. Among the big toe sensors, the normal sensor (T_N) showed a measurable signal, indicating a dominant normal stress in the absence of significant shear. Unexpectedly, the front-tilted sensor (T_F) at the big toe also exhibited a measurable output at 0°, which may be attributed to minor inconsistencies in foot positioning, possibly owing to the participant leaning slightly forward. This could have induced incidental shear stress that was detected by the front-tilted sensor. The other tilted sensors at the toe (T_R, T_L, and T_B) showed

no measurable output, indicating negligible shear stress in these directions under neutral standing conditions.

As the incline increased to 10° and then to 20°, sensor outputs exhibited distinct directional trends. At the big toe, the output from the normal sensor (T_N) gradually decreased. This suggests that the load, which was highly concentrated at the forefoot on a flat surface, began to disperse more broadly across the sole to maintain stability on the incline. Although increased shear stress might be expected, the tilted sensors at the toe (T_R, T_L, T_B, and T_F) continued to show negligible outputs. This is likely attributable to their positioning marginally away from the primary loading zone beneath the toe. Because the toe region is relatively narrow, even small shifts in load could cause the stress to fall outside the effective sensing area of the tilted sensors, limiting their ability to capture shear stress at higher inclines.

Similarly, at the heel, the output from the normal sensor (H_N) decreased with increasing inclination. This observation is consistent with the pressure dispersing from the main contact points; the load initially concentrated at the heel was redistributed across the plantar surface as the posture adapted to the slope. Meanwhile, the tilted heel sensors showed consistent, direction-dependent outputs. Owing to the larger surface area of the heel, sufficient contact was maintained to allow detection of shear stress. Specifically, the right-tilted sensor (H_R) exhibited a gradual decrease in output with increasing slope, indicating a reduction in the normal stress component along the right side of the heel. The left (H_L), front (H_F), and back (H_B) sensors maintained relatively stable outputs across all inclination angles, suggesting consistent shear stress loading in these directions.

Figure 8(c) shows the sensor system's capability to monitor dynamic load shifts during slow in-place walking on a 20° incline. Initially, the right foot was lifted, and no load was detected. As body weight shifted onto the right foot, significant increases in output were recorded by the normal sensors at the toe (T_N) and heel (H_N), indicating normal stress during stance. Additionally, the tilted heel sensors (H_L, H_R, H_B, and H_F) produced noticeable outputs, confirming the presence of measurable directional shear stress. Notably, the output of the right-tilted heel sensor (H_R) was approximately 50% lower than that of the left-tilted sensor (H_L), indicating a shear stress predominantly directed to the left. This directionality is consistent with the inclined posture and confirms the sensor's ability to distinguish shear direction accurately. As the load shifted back to the left foot, sensor outputs from the right foot rapidly returned to zero, demonstrating clear responsiveness and real-time tracking capability.

In summary, these static and dynamic tests confirm that the developed insole sensor modules can effectively distinguish between normal and shear stresses while capturing detailed directional information related to body posture and foot loading. The sensors respond sensitively to changes in standing inclination and weight distribution, making them well-suited for practical biomechanical monitoring applications such as gait analysis, posture correction, and injury prevention in both clinical and athletic contexts.

5.2 Temporal Profiles of Plantar Pressure and Shear Stress during Walking and Running

The dynamic characteristics of the insole sensor were evaluated by measuring temporal changes in plantar pressure (normal stress) and shear stress during walking and running tests. As shown in Fig. 9(a), sensor outputs were recorded at a sampling rate of 100 Hz during walking at 1.25 m/s and running at 2.5 m/s on a flat instrumented treadmill (Instrumented Treadmill, Bertec, USA). Additional tests were conducted under inclined conditions (15° incline at 1.25 m/s walking) to enable comparison between flat and inclined walking scenarios.

The dynamic test results are presented in Figs. 9(b)–(d), showing the temporal outputs of sensor modules located at four anatomical positions: the big toe (T), first metatarsal head (1MH), fifth metatarsal head (5MH), and heel (H). Specifically, the outputs are represented as follows: the normal sensor (N), the difference between right and left tilted sensors (R–L), and the difference between back and front tilted sensors (B–F). In addition, three-axis GRFs, F_x, F_y, and F_z, measured by the treadmill, are plotted simultaneously for validation and comparison with insole sensor outputs. As shown in Figs. 9(b) and 9(c), notable differences were observed between flat and inclined walking. In particular, during inclined walking, the peak output of the heel normal sensor (H_N) decreased by approximately 32%, while the output of the first metatarsal head normal sensor ($1\mathrm{MH}_N$) increased by approximately 120%. These changes reflect a forward redistribution of plantar pressure from the heel toward the forefoot on an inclined surface, consistent with previous plantar pressure studies [33].

The shear stress output from the $1\mathrm{MH}_{B-F}$ sensor also showed significant differences between flat and inclined walking. In flat walking, sequential bidirectional peaks were observed, with magnitudes of approximately 1.32 V (backward) and −0.6 V (forward). In contrast, inclined walking resulted in reversed magnitudes (0.55 V (backward) and −0.92 V (forward)), indicating a reduction in forward-directed shear stress and an increase in backward-directed shear stress. This directional pattern aligns well with the corresponding F_y GRF measurements from the treadmill.

Furthermore, the shear stress profile from the toe region sensor (T_{B-F}) showed consistent bidirectional behavior during both walking conditions. Shear stress was initially

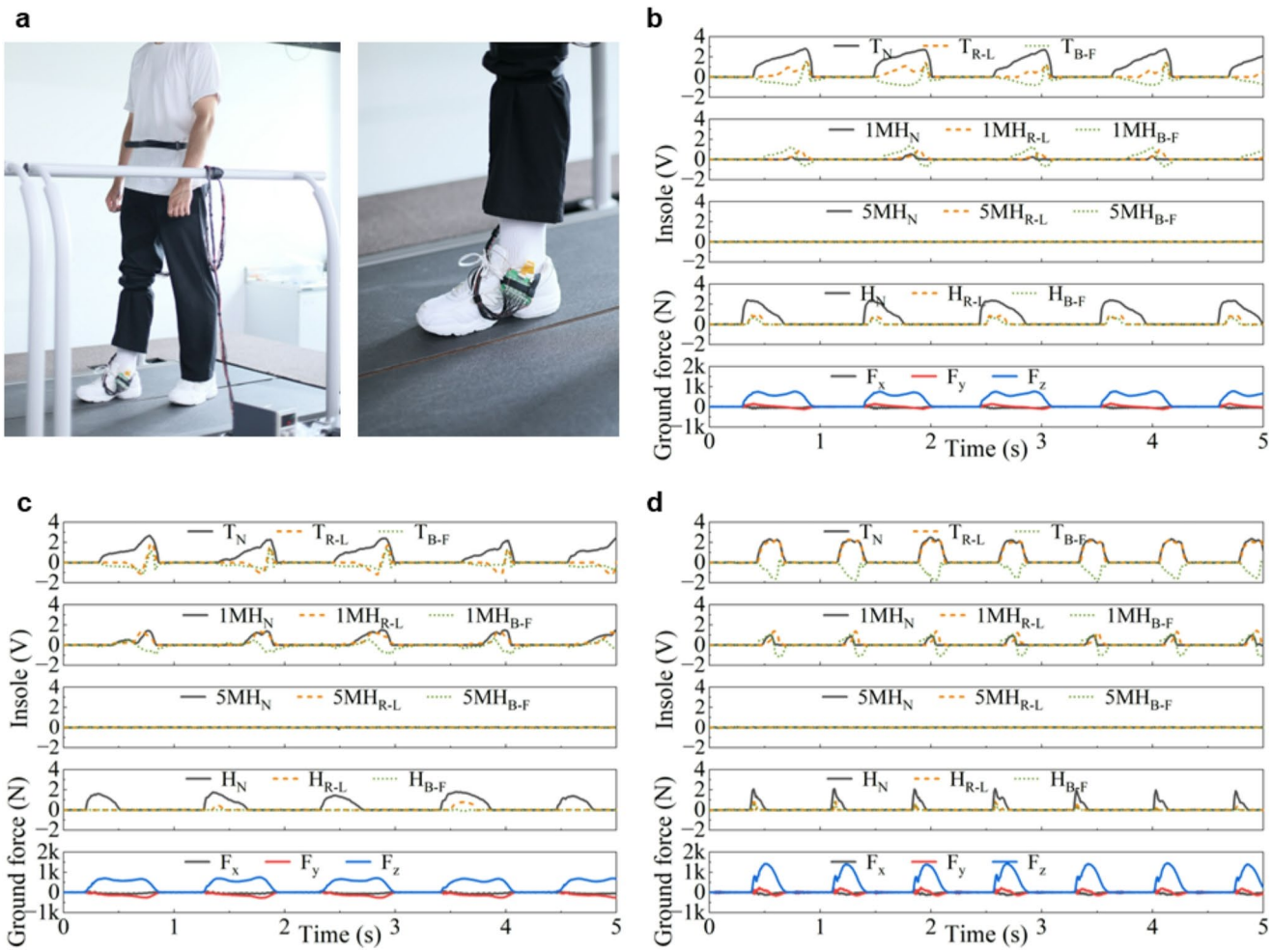


Fig. 9 **a** Photographs of the experimental setup, showing a participant wearing the insole sensor system during treadmill walking and running; **b** insole sensor outputs and GRFs during flat walking at 1.25 m/s; **c** insole sensor outputs and GRFs during 15° inclined walking at 1.25 m/s; **d** insole sensor outputs and GRFs during flat running at 2.5 m/s

directed backward, followed by a forward shift. This pattern likely reflects the big toe's flexible and relatively unconstrained motion during the stance phase, as it moves from heel strike to push-off, producing dynamic shear forces captured by the sensor module.

Figure 9(d) compares sensor outputs during flat running at 2.5 m/s with those during walking at 1.25 m/s. Distinct differences emerge, both in insole sensor signals and GRF data, highlighting changes in foot strike and plantar stress distribution between gait modes. During walking, load transferred from the heel (H_N peak output ≈ 2.4 V) to the toe (T_N peak output ≈ 2.81 V), with minimal loading at the midfoot ($1MH_N$ output ≈ 0.5 V). In contrast, running demonstrated a midfoot strike pattern, with more evenly distributed loading across the foot. Accordingly, sensor outputs showed reduced normal stress at the heel (≈ 2.1 V) and toe (≈ 2.48 V), but a considerable increase in midfoot loading ($1MH_N$ output ≈ 1.1 V).

Shear stress responses during running were also more pronounced and bidirectional. At the midfoot ($1MH_{B-F}$), peak shear stresses of approximately ± 1.06 V were observed, consistent with treadmill F_y force measurements. In the toe region, significant forward-directed shear stress ($T_{B-F} \approx -1.7$ V) was observed, likely indicating that the toe was pulled toward the midfoot during the push-off phase. Additionally, a notable increase in right–left shear stress ($T_{R-L} \approx 2.26$ V) was recorded during running compared to walking. This is attributed to inward foot rotation (toe-in motion), commonly observed in running to stabilize gait, as reported in prior studies [34].

In summary, these dynamic tests demonstrate that integrating normal and shear-stress sensors at key plantar locations enables detailed temporal profiling of plantar loads during various gait conditions. The developed insole sensor module effectively distinguishes between walking and running patterns and accurately captures changes in plantar

pressure and directional shear stresses. This level of detail holds strong potential for precise gait analysis, real-time athletic-performance monitoring, injury prevention, and individualized clinical assessments.

6 Conclusion

In this study, we developed a novel insole sensor system that utilizes conventional piezoresistive pressure sensors to simultaneously measure plantar pressure and shear stress. Multiple sensor modules were strategically positioned at four key plantar regions (big toe, first metatarsal head, fifth metatarsal head, and heel), each comprising one vertically oriented sensor and four tilted sensors, thereby enabling directional sensitivity to shear stress. Vertical and shear compression tests revealed distinct orientation-dependent sensitivities: the vertically oriented sensor (S_N) responded rapidly to low applied pressures (~10 kPa), whereas the tilted sensors exhibited higher response thresholds (200–650 kPa), with their outputs strongly influenced by the direction of loading. FEA further validated these experimental findings by accurately predicting significant nonlinear deformation and orientation changes in the tilted sensors under combined normal and shear loading. This analysis revealed the limitations of conventional linear elasticity assumptions and emphasized the importance of advanced modeling techniques for accurate stress estimation. Static tests conducted at varying incline angles clearly detected load redistribution and directional shear stress variations. Dynamic gait analyses performed during walking and running showed that the sensor outputs closely matched three-axis GRFs, effectively distinguishing walking from running patterns and providing real-time profiles of plantar pressure and shear stress. Despite the successful directional detection of shear stress, achieving precise quantitative measurement remains challenging owing to the inherent cross-sensitivity of piezoresistive sensors to both normal and shear components. Future work should focus on developing specialized piezoresistive sensors that respond exclusively to normal stress, thereby enhancing the accuracy of shear stress measurements. Nevertheless, the developed sensor system offers significant advantages in terms of flexibility, durability, user comfort, and ease of integration into everyday footwear. These features make it highly suitable for applications in biomechanical monitoring, athletic-performance evaluation, injury prevention, and personalized clinical assessments.

Acknowledgements This research was supported by the Chung-Ang University research grant in 2022 and by the Technology Innovation Program (or Industrial Strategic Technology Development Program) (20007058, Development of safe and comfortable human augmentation hybrid robot suit) funded By the Ministry of Trade, Industry & Energy (MOTIE, Korea).

Funding Open Access funding enabled and organized by Chung-Ang University

Open Access This article is licensed under a Creative Commons Attribution 4.0 International License, which permits use, sharing, adaptation, distribution and reproduction in any medium or format, as long as you give appropriate credit to the original author(s) and the source, provide a link to the Creative Commons licence, and indicate if changes were made. The images or other third party material in this article are included in the article's Creative Commons licence, unless indicated otherwise in a credit line to the material. If material is not included in the article's Creative Commons licence and your intended use is not permitted by statutory regulation or exceeds the permitted use, you will need to obtain permission directly from the copyright holder. To view a copy of this licence, visit http://creativecommons.org/licenses/by/4.0/.

References

1. Yalçın, N., Esen, E., Kanatli, U., & Yetkin, H. (2010). Evaluation of the medial longitudinal arch: A comparison between the dynamic plantar pressure measurement system and radiographic analysis. *Acta Orthopaedica Et Traumatologica Turcica*, *44*(3), 241–245.
2. Bus, A. S., Akkerman, M. E., & Maas, M. (2021). Changes in sub-calcaneal fat pad composition and their association with dynamic plantar foot pressure in people with diabetic neuropathy. *Clinical Biomechanics*, *88*, 105441.
3. Gao, Z. X., Mei, Q. C., Xiang, L. L., Baker, J. S., Fernandez, J., & Gu, Y. D. (2022). Effects of limb dominance on the symmetrical distribution of plantar loading during walking and running. *Proceedings of the Institution of Mechanical Engineers Part P-Journal of Sports Engineering and Technology*, 236(1), 17–23.
4. Honert, E. C., Hoitz, F., Blades, S., Nigg, S. R., & Nigg, B. M. (2022). Estimating running ground reaction forces from plantar pressure during graded running. *Sensors (Basel, Switzerland)*, *22*(9), 3338.
5. Queen, R. M., Haynes, B. B., Hardaker, W. M., & Garrett, W. E. (2007). Forefoot loading during 3 athletic tasks. *American Journal of Sports Medicine*, *35*(4), 630–636.
6. Hu, S. T., Li, H. R., Lu, W. H., Han, T. Y., Xu, Y. Z., Shi, X., Peng, Z. K., & Cao, X. B. (2024). Triboelectric insoles with Normal-Shear plantar stress perception. *Advanced Functional Materials*, *34*(16), 2313458.
7. Ramirez-Bautista, J. A., Hernández-Zavala, A., Chaparro-Cárdenas, S. L., & Huerta-Ruelas, J. A. (2018). Review on plantar data analysis for disease diagnosis. *Biocybernetics and Biomedical Engineering*, *38*(2), 342–361.
8. Zheng, Q., Dai, X., Wu, Y., Liang, Q., Wu, Y., Yang, J., Dong, B., Gao, G., Qin, Q., & Huang, L. B. (2023). Self-powered high-resolution smart insole system for plantar pressure mapping. *BMEMat*, 1(1), e12008.
9. Jones, A. D., De Siqueira, J., Nixon, J. E., Siddle, H. J., Culmer, P. R., & Russell, D. A. (2022). Plantar shear stress in the diabetic foot: A systematic review and meta-analysis. *Diabetic Medicine*, 39(1), e14661.
10. Zhang, X. Y., Li, B., Liang, K. Y., Wan, Q. F., & Vanwanseele, B. (2016). An optimized design of in-shoe heel lifts reduces plantar pressure of healthy males. *Gait & Posture*, *47*, 43–47.
11. Binelli, M. R., van Dommelen, R., Nagel, Y., Kim, J., Haque, R. I., Coulter, F. B., Siqueira, G., Studart, A. R., & Briand, D. (2023). Digital manufacturing of personalised footwear with embedded sensors. *Scientific Reports*, 13(1), 1962.

12. Bader, D. L., & Worsley, P. R. (2018). Technologies to monitor the health of loaded skin tissues. *Biomedical Engineering Online*, *17*(1), 40.
13. Tang, J. H., Bader, D. L., Moser, D., Parker, D. J., Forghany, S., Nester, C. J., & Jiang, L. D. (2023). A wearable insole system to measure plantar pressure and shear for people with diabetes. *Sensors (Basel, Switzerland)*, *23*(6), 3126.
14. Mori, T., Hamatani, M., Noguchi, H., Oe, M., & Sanada, H. (2012). Insole-Type simultaneous measurement system of plantar pressure and shear force during gait for diabetic patients. *Journal of Robotics and Mechatronics*, *24*(5), 766–772.
15. Cong, Y., Lam, W. K., Cheung, J. T. M., & Zhang, M. (2014). In-shoe plantar tri-axial stress profiles during maximum-effort cutting maneuvers. *Journal of Biomechanics*, *47*(16), 3799–3806.
16. Heracleous, C., Leong, J. J. H., & Loureiro, R. C. V. (2023). Development of a Low-Profile planar sensor for the detection of normal and shear forces. *IEEE Journal on Flexible Electronics*, *2*(2), 160–167.
17. Wang, L. F., Jones, D., Chapman, G. J., Siddle, H. J., Russell, D. A., Alazmani, A., & Culmer, P. (2020). A review of wearable sensor systems to monitor plantar loading in the assessment of diabetic foot ulcers. *IEEE Transactions on Biomedical Engineering*, *67*(7), 1989–2004.
18. Claver, U. P., & Zhao, G. (2021). Recent progress in flexible pressure sensors based electronic skin. *Advanced Engineering Materials*, *23*(5), 2001187.
19. Li, J., Bao, R., Tao, J., Peng, Y., & Pan, C. (2018). Recent progress in flexible pressure sensor arrays: From design to applications. *Journal of Materials Chemistry C*, *6*(44), 11878–11892.
20. Xu, C., Chen, J., Zhu, Z., Liu, M., Lan, R., Chen, X., Tang, W., Zhang, Y., & Li, H. (2024). Flexible pressure sensors in human–machine interface applications. *Small (Weinheim an Der Bergstrasse, Germany)*, *20*(15), 2306655.
21. Qin, R., Nong, J., Wang, K., Liu, Y., Zhou, S., Hu, M., Zhao, H., & Shan, G. (2024). Recent advances in flexible pressure sensors based on MXene materials. *Advanced Materials*, *36*(24), 2312761.
22. Tavares, C., Domingues, M. F., Frizera-Neto, A., Leite, T., Leitão, C., Alberto, N., Marques, C., Radwan, A., Rocon, E., André, P., & Antunes, P. (2018). Gait shear and plantar pressure monitoring: A non-invasive OFS based solution for e-health architectures. *Sensors (Basel, Switzerland)*, *18*(5), 1334.
23. Pan, L., Chortos, A., Yu, G., Wang, Y., Isaacson, S., Allen, R., Shi, Y., Dauskardt, R., & Bao, Z. (2014). An ultra-sensitive resistive pressure sensor based on hollow-sphere microstructure induced elasticity in conducting polymer film. *Nature Communications*, *5*(1), 3002.
24. Fiorillo, A. S., Critello, C. D., & Pullano, S. A. (2018). Theory, technology and applications of piezoresistive sensors: A review. *Sensors and Actuators A: Physical*, *281*, 156–175.
25. Shang, S., Yue, Y., & Wang, X. (2016). Piezoresistive strain sensing of carbon black/silicone composites above percolation threshold. *Review of Scientific Instruments*, *87*(12), 123910.
26. Mishra, R. B., El-Atab, N., Hussain, A. M., & Hussain, M. M. (2021). Recent progress on flexible capacitive pressure sensors: From design and materials to applications. *Advanced Materials Technologies*, *6*(4), 2001023.
27. Lee, Y. R., Chung, J., Oh, Y., & Cha, Y. (2019). Flexible shear and normal force sensor using only one layer of polyvinylidene fluoride film. *Applied Sciences*, *9*(20), 4339.
28. Gao, S., Chen, J. L., Dai, Y. N., Wang, R., Kang, S. B., & Xu, L. J. (2021). Piezoelectric-Based insole force sensing for gait analysis in the internet of health things. *IEEE Consumer Electronics Magazine*, *10*(1), 39–44.
29. Yang, P., Shi, Y. X., Li, S. Y., Tao, X. L., Liu, Z. Q., Wang, X. L., Wang, Z. L., & Chen, X. Y. (2022). Monitoring the degree of comfort of shoes In-Motion using triboelectric pressure sensors with an ultrawide detection range. *Acs Nano*, *16*(3), 4654–4665.
30. Tavares, C., Leite, F., Domingues, M. D., Paixao, T., Alberto, N., Ramos, A., Silva, H., & Antunes, P. F. D. (2021). Optically instrumented insole for gait plantar and shear force monitoring. *Ieee Access : Practical Innovations, Open Solutions*, *9*, 132480–132490.
31. Wang, L. F., Jones, D., Jones, A., Chapman, G. J., Siddle, H. J., Russell, D., Alazmani, A., & Culmer, P. R. (2022). A portable insole system to simultaneously measure plantar pressure and shear stress. *IEEE Sensors Journal*, *22*(9), 9104–9113.
32. ., Dassault Systèmes Simulia Corp, User's, A. B. A. Q. U. S., & Manual Ver. 6.13, Dassault Systèmes Simulia Corp., Providence, RI, USA.
33. Ho, I. J., Hou, Y. Y., Yang, C. H., Wu, W. L., Chen, S. K., & Guo, L. Y. (2010). Comparison of plantar pressure distribution between different speed and incline during treadmill jogging. *Journal of Sports Science and Medicine*, *9*(1), 154–160.
34. Guo, L. Y., Su, F. C., Yang, C. H., Wang, S. H., Chang, J. J., Wu, W. L., & Lin, H. T. (2006). Effects of speed and incline on lower extremity kinematics during treadmill jogging in healthy subjects. *Biomedical Engineering-Applications Basis Communications*, *18*(2), 73–79.

Publisher's Note Springer Nature remains neutral with regard to jurisdictional claims in published maps and institutional affiliations.



Seyong Jung received his B.S. degree in Mechanical Engineering from University of Ulsan, Ulsan, Republic of Korea, in 2023. He is currently a M.S. degree candidate in Chung-Ang University, Seoul, Republic of Korea. His current research interests include development of insole sensors for measuring plantar shear stress and pressure using piezoresistive sensors.



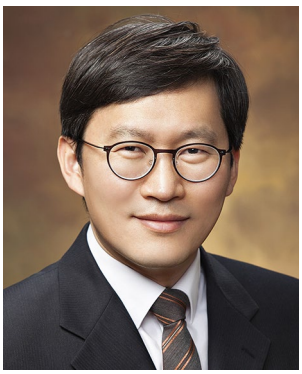
Quang Van Duong received his B.E. degree in Materials Engineering, Hanoi University of Science and Technology, Hanoi, Vietnam, in 2014. In 2021, he received his Ph.D. degree in Mechanical Engineering from Chung-Ang University, Seoul, Republic of Korea. Since 2021, he has been Postdoctoral Researcher at Department of Mechanical Engineering, Chung-Ang University. His current research interests are the development of soft sensors and actuators based on ferroelectric polymers.



Juntae Kim received his B.S. degree in Electrical and Computer Engineering from The Ohio State University, Columbus, OH, USA, in 2012, and his M.S. degree in Electrical Engineering from the University of Southern California, Los Angeles, CA, USA, in 2013. Since 2018, he has served as CEO of Polyworks, leading the development of film-type sensors and their driving circuits. His current research interests include film-type sensors and the advancement of associated driving circuit technologies.



Giuk Lee received the B.S. and Ph.D. degrees in Mechanical and Aerospace Engineering from Seoul National University, South Korea, in 2010 and 2014, respectively. He was a postdoctoral fellow at the Korea Institute of Science and Technology, and later at Harvard University, USA. He is currently an Associate Professor in the School of Mechanical Engineering at Chung-Ang University, Seoul, Republic of Korea, where he directs the Assistive and Rehabilitation Robotics Lab and the Human-Robot Convergence Research Center. He is also the founder and CEO of HUROTICS Inc. His research interests include wearable robotics, soft exosuits, human-in-the-loop optimization, and rehabilitation engineering.



Seung Tae Choi received the B.S. degree in mechanical design and precision engineering from Chung-Ang University, Seoul, Republic of Korea, in 1995, and the M.S. and Ph.D. degrees in mechanical engineering from Korea Advanced Institute of Science and Technology, Daejeon, Republic of Korea, in 1997 and 2002, respectively. He is currently a Professor in the School of Mechanical Engineering. His current research interests include multiscale analysis of deformation and fracture of polycrystalline materials and development of ferroelectric polymer sensors and actuators.